Power Transfer Through Strongly Coupled Resonances

by

André Kurs

Submitted to the Department of Physics
in partial fulfillment of the requirements for the degree of

Master of Science in Physics

at the

MASSACHUSETTS INSTITUTE OF TECHNOLOGY

September 2007

Author .....
Department of Physics
August 10, 2007

Certified by .....
Marin Soljačić
Assistant Professor of Physics
Thesis Supervisor

Accepted by .....
Thomas J. Greytak
Associate Department Head for Education

Power Transfer Through Strongly Coupled Resonances

by

André Kurs

Submitted to the Department of Physics
on August 10, 2007, in partial fulfillment of the
requirements for the degree of
Master of Science in Physics

Abstract

Using self-resonant coils in a strongly coupled regime, we experimentally demonstrate efficient non-radiative power transfer over distances of up to eight times the radius of the coils. We use this system to transfer 60W with approximately 45% efficiency over distances in excess of two meters. We present a quantitative model describing the power transfer which matches the experimental results to within 5%, and perform a finite element analysis of the objects used. We finally discuss the robustness of the mechanism proposed and consider safety and interference concerns.

Thesis Supervisor: Marin Soljačić
Title: Assistant Professor of Physics

Acknowledgments

I would like to thank all my collaborators on this project: Aristeidis Karalis, Robert Moffatt, Prof. John D. Joannopoulos, Prof. Peter Fisher, and Prof. Marin Soljačić. It has been a pleasure to work with all them. I would like to doubly thank my advisor, Marin Soljačić, for letting me work on this project, for all his support, and for his help in the laboratory during the final stretch of measurements.

My thanks also go to Mike Grossman for his help with machining, Ivan Čelanović for helping with the electronics, Zheng Wang for his assistance with COMSOL, and to Mark Rudner for useful discussions.

Contents

List of Figures

List of Tables

Chapter 1

Introduction

At the turn of the 20th century, Nikola Tesla [1, 2, 3] devoted much effort to developing a system for transferring large amounts of power over continental distances. His main goal was to bypass the electrical-wire grid, but for a number of technical and financial difficulties, this project was never completed. Moreover, typical embodiments of Tesla's power transfer scheme (e.g., Tesla coils) involve extremely large electric fields and are potential safety hazards. The past decade has witnessed a dramatic surge in the use of autonomous electronic devices (laptops, cell-phones, robots, PDAs, etc) whose batteries need to be constantly recharged. As a consequence, interest in wirelessly recharging or powering such devices has reemerged [4, 5, 6]. Our attempts to help to fulfill this need led us to look for physical phenomena that would enable a source and a device to exchange energy efficiently over mid-range distances, while dissipating relatively little energy in extraneous objects. By mid-range, we mean that the separation between the two objects effecting the transfer should be of the order of a few times the characteristic sizes of the objects. Thus, for example, one source could be used to power or recharge all portable devices within an average-sized room.

A natural candidate for wirelessly transferring powering over mid-range or longer distances would be to use electromagnetic radiation. But radiative transfer [7], while perfectly suitable for transferring information, poses a number of difficulties for power transfer applications: the efficiency of power transfer is very low if the radiation is omnidirectional (since the power captured is proportional to the cross-section of the

receiving antenna, and most of the power is radiated in other directions), and requires an uninterrupted line of sight and sophisticated tracking mechanisms if radiation is unidirectional (which might also damage anything that interrupts the line of sight).

An alternative approach, which we pursue here, is to exploit some near-field interaction between the source and the device, and somehow tune this system so that efficient power transfer is possible. A recent theoretical paper [8] presented a detailed analysis of the feasibility of using resonant objects coupled through their near-fields to achieve mid-range energy transfer. The basic idea is that in systems of coupled resonances (e.g. acoustic, electro-magnetic, magnetic, nuclear), there may be a general strongly coupled regime of operation [9]. It is a general physical property that if one can operate in this regime in a given system, the energy transfer is expected to be very efficient. Mid-range power transfer implemented this way can be nearly omnidirectional and efficient, irrespective of the geometry of the surrounding space, and with low losses into most off-resonant environmental objects [8].

The above considerations apply irrespective of the physical nature of the resonances. In the current work, we focus on one particular physical embodiment: magnetic resonances [10], meaning that the interaction between the objects occurs predominantly through the magnetic fields they generate. Magnetic resonances are particularly suitable for everyday use because biological tissue and most common materials do not interact strongly with magnetic fields, which helps make the system safer and more efficient. We were able to identify the strongly coupled regime in the system of two coupled magnetic resonances by exploring non-radiative (near-field) magnetic resonant induction at MHz frequencies. At first glance, such power transfer is reminiscent of the usual magnetic induction [11]; however, note that the usual non-resonant induction is very inefficient unless the two coils share a core with high magnetic permeability or are very close to each other. Moreover, operating on resonance is necessary but not sufficient to achieve good efficiency at mid-range distances. Indeed, Tesla's pioneering work made extensive use of resonant induction, and many technologies available today (e.g., radio receivers, RFID tags, and cochlear implants [12]) also rely on resonance, yet their efficiencies are not very good at mid-

range distances. Operation in the strong-coupling regime, for which resonance is a precondition, is what makes the power transfer efficient.

The work presented in this thesis was done in collaboration with Aristeidis Karalis, Robert Moffatt, Prof. J. D. Joannopoulos, Prof. Peter Fisher, and Prof. Marin Soljačić. Our main results were published in the July 6th 2007 issue of *Science* [13].

Chapter 2

Theory of strongly coupled systems

2.1 Motivation and basics

In order to achieve efficient power transfer, it pays to have a methodical way of tuning the parameters of a given system (such as its geometry, the materials used, and the resonant frequency) so that it operates in the strongly coupled regime. In some cases, this analysis can be done directly in term of familiar quantities. For instance, when dealing with coupled LCR systems that are composed of lumped elements to a good approximation, one can solve the circuit equations directly and work exclusively with regular inductances, capacitances, and resistances. Our experimental system, however, consists of self-resonant coils which rely on distributed capacitances and inductances to achieve resonance, and cannot easily be analyzed in terms of lumped elements. In contrast, coupled-mode theory [14] provides a simple yet accurate way of modeling this system, and gives a more intuitive understanding of what makes power transfer efficient in the strongly coupled regime.

The essence of coupled-mode theory is to reduce the analysis of a general physical system to the solution of the following set of coupled differential equations:

$$\dot{a}_m(t) = -(i\omega_m - i\Gamma_m)a_m(t) - \sum_{n \neq m} i\kappa_{mn}a_n(t) + F_m(t), \tag{2.1}$$

where the indices denote the different resonant objects. The variables $a_m(t)$ are de-

fined so that the energy contained in object m is $|a_m(t)|^2$, ω_m is the resonant frequency of that isolated object, and Γ_m is its intrinsic decay rate (e.g. due to absorption and radiated losses). Thus, in this framework the variable $a_0(t)$ corresponding to an uncoupled and undriven oscillator with parameters ω_0 and Γ_0 would evolve in time as $e^{-i\omega_0 t-\Gamma_0 t}$. The κ_{mn} are coupling coefficients between the resonant objects indicated by the subscripts, and $F_m(t)$ are driving terms.

The first assumption of coupled-mode theory is that the range of frequencies of interest is sufficiently narrow that the phenomenological parameters in Eq. 2.1 can be treated as constants and the coupled differential equations can be treated as linear. The second is that the overall field profile can be described as a superposition of the modes due to each object. The second condition usually implies that the interaction between the resonators must not be strong enough so as to significantly distort the individual eigenmodes. In that sense, the "strong" in "strong-coupling regime" is a relative term, one that we will make more precise below.

We limit our treatment to at most two objects. We denote them by source (identified by the subscript S) and device (subscript D). The coupling coefficients κ_{SD} and κ_{DS} are not independent. Indeed, an undriven system consisting of these two objects would lose energy at the rate

$$\begin{aligned}\frac{d}{dt}\left(|a_S|^2+|a_D|^2\right) &= a_S\dot{a}_S^*+\dot{a}_S a_S^*+a_D\dot{a}_D^*+\dot{a}_D a_D^* \\ &= -2\Gamma_S|a_S|^2-2\Gamma_D|a_D|^2 \\ &- i\left(\kappa_{SD}a_S^*a_D-\kappa_{SD}^*a_Sa_D^*+\kappa_{DS}a_Sa_D^*-\kappa_{DS}^*a_S^*a_D\right), \quad (2.2)\end{aligned}$$

where we plugged in Eq. 2.1 between the first and second lines. Since the only mechanisms through which the system can lose energy are incorporated in Γ_S and Γ_D, the third line in Eq. 2.2 must equal 0. Moreover, the phases of a_S and a_D are arbitrary, and we find that κ_{SD} and κ_{DS} are real and equal. Clearly, this property holds for all the κ_{mn} used in Eq. 2.1. We shall henceforth use the single coupling coefficient $\kappa=\kappa_{SD}=\kappa_{DS}$. Eq. 2.2 also indicates that κ is related to the transfer of energy between the two oscillators, and we shall use that property below to theoretically

derive κ for our experimental system.

2.2 Single oscillator driven at constant frequency

For a single driven oscillator at steady-state, Eq. 2.1 reduces to

$$\dot{a}(t) = -i(\omega_0 - i\Gamma)a + Fe^{-i\omega t}, \tag{2.3}$$

where $Fe^{-i\omega t}$ is the steady-state driving term. The solution is

$$a_S(t) = \frac{Fe^{-i\omega t}}{i(\omega_0 - \omega) + \Gamma}. \tag{2.4}$$

One way to measure Γ_S experimentally is to drive the oscillator at steady-state and determine the frequency width $\Delta\omega$ for which the amplitude of the oscillation is greater than $1/\sqrt{2}$ of the peak amplitude (which occurs at $\omega = \omega_S$). From Eq. 2.4 we find that $2\Gamma = \Delta\omega$. It is also convenient to work with the dimensionless quality factor Q defined as

$$\begin{aligned} Q &= 2\pi \frac{\langle \text{energy stored} \rangle}{\langle \text{power dissipated per cycle} \rangle} \\ &= \frac{\omega_0}{2\Gamma} \\ &= \frac{\omega_0}{\Delta\omega}. \end{aligned} \tag{2.5}$$

That is, in one period of oscillation a resonant object loses $1/Q$ of its energy.

2.3 Two coupled oscillators

We now solve the coupled-mode equations in two different cases: undriven and driven. The undriven result is useful for extracting κ from computer simulations of the system, while the driven result allows us to determine κ from experiment.

The system of equations for the undriven case is

$$\begin{aligned} \dot{a}_S &= -i(\omega_S - i\Gamma_S)a_S - i\kappa a_D \\ \dot{a}_D &= -i(\omega_D - i\Gamma_D)a_D - i\kappa a_S. \end{aligned} \tag{2.6}$$

This has solutions with eigenfrequencies

$$\begin{aligned} \omega_{1,2} &= \frac{1}{2}\left[\omega_S + \omega_D - i\left(\Gamma_S + \Gamma_D\right)\right] \\ &\pm \frac{1}{2}\left[4\kappa^2 + (\omega_S - \omega_D)^2 - (\Gamma_S - \Gamma_D)^2 - 2i(\Gamma_S - \Gamma_D)(\omega_S - \omega_D)\right]^{1/2}. \end{aligned} \tag{2.7}$$

For the case of two identical oscillators with $\omega_S = \omega_D = \omega_0$ and $\Gamma_S = \Gamma_D = \Gamma$, this simplifies to

$$\omega_{1,2} = \omega_0 - i\Gamma \pm \kappa. \tag{2.8}$$

Thus we see that κ is related to the splitting between the eigenfrequencies by $2\kappa = \omega_1 - \omega_2$.

The driven case adds a term $Fe^{-i\omega t}$ to the first line of Eq. 2.6. The solution to the new system of coupled equations is

$$\begin{aligned} a_S &= \frac{\left[\Gamma_D - i(\omega - \omega_D)\right] Fe^{-i\omega t}}{\kappa^2 + \Gamma_S\Gamma_D - (\omega_S - \omega)(\omega_D - \omega) + i\left[\Gamma_S(\omega_D - \omega) + \Gamma_D(\omega_S - \omega)\right]} \\ a_D &= \frac{-i\kappa F e^{-i\omega t}}{\kappa^2 + \Gamma_S\Gamma_D - (\omega_S - \omega)(\omega_D - \omega) + i\left[\Gamma_S(\omega_D - \omega) + \Gamma_D(\omega_S - \omega)\right]}. \end{aligned} \tag{2.9}$$

Our measurement of κ involves measuring the amplitude of the excitation at the device object while sweeping the driving frequency ω. Restricting ourselves to the case of two identical oscillators, the two peaks in the amplitude occur at

$$\omega'_{1,2} = \omega_0 \pm \sqrt{\kappa^2 - \Gamma^2}. \tag{2.10}$$

κ is therefore obtained by measuring Γ and the frequency splitting between the two peaks.

2.4 Transferring power

Once the device is excited by the source (which is in turn driven at constant frequency), we can extract energy and convert it into useful work by adding a load (denoted by the subscript W) to the device. In the particular case of electromagnetic resonances, the load effectively acts as a circuit resistance connected to the device. More generally, the load has the effect of contributing an additional term to the unloaded device object's Γ_D. The total decay rate at the device is therefore changed to $\Gamma'_D = \Gamma_D + \Gamma_W$, where Γ_D is the device's intrinsic decay rate, as before. The work extracted is determined by the power dissipated in the load, i.e. $2\Gamma_W|a_D(t)|^2$ and the overall efficiency of the system is

$$\begin{aligned} \eta &= \frac{\Gamma_W|a_D|^2}{\Gamma_S|a_S|^2 + (\Gamma_D + \Gamma_W)|a_D|^2} \\ &= \frac{\Gamma_W\kappa^2}{\Gamma_S[(\Gamma_D + \Gamma_W)^2 + (\omega - \omega_D)]^2 + (\Gamma_D + \Gamma_W)\kappa^2}, \end{aligned} \tag{2.11}$$

where we plugged in Eq. 2.9 when going from the first to the second line. We can tell by inspection that the efficiency is maximized when $\omega = \omega_D$.[1] Eq. 2.11 then simplifies to

$$\eta = \frac{(\Gamma_W/\Gamma_D)\kappa^2/(\Gamma_S\Gamma_D)}{[1 + \Gamma_W/\Gamma_D]\kappa^2/(\Gamma_S\Gamma_D) + [1 + \Gamma_W/\Gamma_D]^2}. \tag{2.12}$$

Maximizing the efficiency is now equivalent to solving and impedance matching problem: given the intrinsic parameters of the system, which load Γ_W maximizes η? Maximizing Eq. 2.12 yields the optimal value $\Gamma_W = \Gamma_D\sqrt{1 + \kappa^2/\Gamma_S\Gamma_D}$.

We have found that the efficiency of power transfer depends solely on the dimensionless parameter $\kappa/\sqrt{\Gamma_S\Gamma_D}$. Fig. 2-1 shows that the transfer is efficient (i.e. η is

[1] For electromagnetic systems, an intuitive way of arriving at this result is to note that the power dissipated by each object is proportional to the square of the amplitude of the electromagnetic fields that it generates, while the power transferred between the source and the device is represented by the time-averaged Poynting vector $\langle \mathbf{P} \rangle = \frac{1}{2}\mathrm{Re}\,[\mathbf{E} \times \mathbf{H}^*]$. Since the electric and magnetic fields generated by a resonant object are $\pi/2$ out of phase, the time-averaged Poynting vector between source and device is maximized when there is a $\pi/2$ phase difference between the two objects. We see from Eq. 2.9 that this occurs when $\omega = \omega_D$.

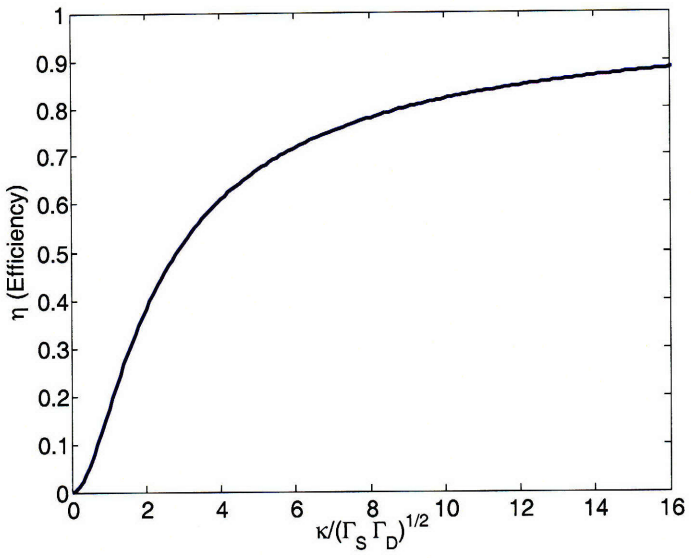

Figure 2-1: Efficiency as a function of the parameter $\kappa/\sqrt{\Gamma_S\Gamma_D}$. In the vicinity of $\kappa/\sqrt{\Gamma_S\Gamma_D} \simeq 1$, the efficiency rises sharply, thus justifying the criterion $\kappa/\sqrt{\Gamma_S\Gamma_D} \gtrsim 1$ for efficient power transfer.The efficiency curve asymptotes to 1 as $\kappa/\sqrt{\Gamma_S\Gamma_D} \to \infty$.

of order 1) when $\kappa/\sqrt{\Gamma_S\Gamma_D} \gtrsim 1$. This is what we denote as the strongly coupled regime. An intuitive way of understanding why power transfer is efficient in this regime is to note that $\sqrt{\Gamma_S\Gamma_D}$ is essentially the rate at which the source and device dissipate energy, while κ is a measure of how fast the two objects exchange energy. If $\kappa \gtrsim \sqrt{\Gamma_S\Gamma_D}$, then the energy travels from the source to the device before too much of it gets wasted away.

Note that the results of this chapter apply to all physical systems of coupled resonators. We now turn our attention to the system of self-resonant electromagnetic coils which we used to demonstrate experimentally the principle of strong-coupling and efficient power transfer.

Chapter 3

Analytical model for self-resonant coils

3.1 Description of self-resonant coils

Our experimental realization of the power transfer scheme consists of two identical self-resonant coils made of an electrically conducting wire of total length l and cross-sectional radius a wound into a helix of n turns, radius r, and height h. To the best of our knowledge, there is no exact electromagnetic solution for a conducting helix of finite length in the literature, and even in the case of infinitely long coils, the results rely on assumptions that are inadequate for our system [15]. We have found, however, that a simple quasi-static model is in good agreement (approximately 5%) with experiment. We have also tried to model the coils computationally using a finite-element software package [16] but given the limited computational resources at our disposal, we have been unable to extract all the parameters needed for a full coupled-mode theory treatment. In this chapter, we present the analytical model, while the computational analysis is described in the next.

3.2 Assumptions of the analytical model

We start by observing that the current has to be zero at the ends of the coil, and make the educated guess that the resonant modes of the coil are well approximated by sinusoidal current profiles along the length of the conducting wire. We are interested in the lowest mode, so if we denote by s the parameterization coordinate along the length of the conductor, such that it runs from $-l/2$ to $+l/2$, then the time-dependent current profile has the form $I_0 \cos(\pi s/l)e^{-i\omega_0 t}$. Using the continuity equation for charge

$$\frac{\partial \rho}{\partial t} + \nabla \cdot \mathbf{J} = 0 \tag{3.1}$$

(where ρ is the charge density and $\mathbf{J}$ is the current density) we find that the linear charge density profile is of the form $\lambda_0 \sin(\pi s/l)e^{-i\omega t}$, so that one-half of the coil (when sliced perpendicularly to its axis) contains an oscillating total charge (of amplitude $q_0 = \lambda_0 l/\pi$) that is equal in magnitude but opposite in sign to the charge in the other half.

3.3 Resonant frequency

As the coil is resonant, the current and charge density profiles are $\pi/2$ out of phase from each other, meaning that the real part of one is maximum when the real part of the other is zero. Equivalently, the energy contained in the coil is at certain points in time completely due to the current, and at other points, completely due to the charge. Using electromagnetic theory, we can define an effective inductance L and an effective capacitance C for each coil as follows:

$$L = \frac{\mu_0}{4\pi |I_0|^2} \int\int d\mathbf{r} d\mathbf{r}' \frac{\mathbf{J}(\mathbf{r}) \cdot \mathbf{J}(\mathbf{r}')}{|\mathbf{r} - \mathbf{r}'|}, \tag{3.2}$$

$$\frac{1}{C} = \frac{1}{4\pi \epsilon_0 |q_0|^2} \int\int d\mathbf{r} d\mathbf{r}' \frac{\rho(\mathbf{r})\rho(\mathbf{r}')}{|\mathbf{r} - \mathbf{r}'|}, \tag{3.3}$$

where the spatial current $\mathbf{J}(\mathbf{r})$ and charge density $\rho(\mathbf{r})$ are obtained respectively from the current and charge densities along the isolated coil, in conjunction with the geometry of the object. One can then compute L and C by numerical integration. As defined, L and C have the property that the energy U contained in the coil is given by

$$\begin{aligned} U &= \frac{1}{2}L|I_0|^2 \\ &= \frac{1}{2C}|q_0|^2. \end{aligned} \tag{3.4}$$

Given this relation and the equation of continuity, one finds that the resonant frequency is $f_0 = 1/2\pi\sqrt{LC}$. We can now treat this coil as a standard oscillator in coupled-mode theory by defining $a(t) = \sqrt{L/2}I_0(t)$.

3.4 Losses

In this model, the coils dissipate energy through two mechanisms: ohmic (resistive) losses and radiation. At MHz frequencies, the electrical current in a typical metal flows within a few tens of micrometers of the surface of the conductor because of the skin effect [17]. For a *uniform* current flowing through a cylindrical conductor of conductivity σ, cross-sectional radius a, length l, and skin depth $\sqrt{2/\mu_0\sigma\omega}$, the ohmic resistance would be $R_o' = l/2\pi\sigma a\delta = \sqrt{\mu_0\omega/2\sigma}(l/2\pi a)$. Our model assumes a sinusoidal current distribution such that the spatial average of the amplitude-squared is $|I_0|^2/2$. If we define the ohmic resistance R_o for our coil's non-uniform current distribution such that the resistive losses equal $R_o|I_0|^2/2$, then

$$R_o = \sqrt{\frac{\mu_0\omega}{2\sigma}}\frac{l}{4\pi a} \tag{3.5}$$

We may decompose the radiation emitted by the coil into two terms. One of them is roughly a magnetic dipole term due to the current flowing around in loops, the

other is an electric dipole term created by the oscillating charge along the axis of the coil. The far-fields created by each term have different polarizations and do not interfere. Therefore the total power radiated is just the sum of the powers radiated by each term. Proceeding as in the case of the ohmic resistance, we modify the standard formulas for magnetic and electric dipole radiation and obtain

$$R_r = \sqrt{\frac{\mu_0}{\epsilon_0}} \left(\frac{\pi}{12} n^2 \left(\frac{\omega r}{c} \right)^4 + \frac{2}{3\pi^3} \left(\frac{\omega h}{c} \right)^2 \right). \tag{3.6}$$

The first term in Eq. 3.6 is the radiation due to the magnetic dipole and the second is that due to the electric dipole. We can now compute the coupled-mode theory decay constant for the coil as $\Gamma = (R_o + R_r)/2L$, and the associated quality factor is $Q = \omega_0/2\Gamma$. For later comparison with the computational finite-element results, it is convenient to define ohmic and radiative Q's: $Q_o = \omega_0 L/R_o$ and $Q_r = \omega_0 L/R_r$. These two are related to the overall Q by $Q^{-1} = Q_o^{-1} + Q_r^{-1}$.

3.5 Coupling coefficient between two coils

We find the coupling coefficient κ_{DS} by looking at the power transferred from the source to the device coil, assuming a steady-state solution in which currents and charge densities vary in time as $e^{-i\omega_0 t}$.

$$\begin{aligned} P_{DS} &= \int d\mathbf{r} \mathbf{E}_S(\mathbf{r}) \cdot \mathbf{J}_D(\mathbf{r}) \\ &= -\int d\mathbf{r} \left(\dot{\mathbf{A}}_S(\mathbf{r}) + \nabla \phi_S(\mathbf{r}) \right) \cdot \mathbf{J}_D(\mathbf{r}) \\ &= -\frac{1}{4\pi} \int \int d\mathbf{r} d\mathbf{r}' \left(\mu_0 \frac{\dot{\mathbf{J}}_S(\mathbf{r}')}{|\mathbf{r}' - \mathbf{r}|} + \frac{\rho_S(\mathbf{r}')}{\epsilon_0} \frac{\mathbf{r}' - \mathbf{r}}{|\mathbf{r}' - \mathbf{r}|^3} \right) \cdot \mathbf{J}_D(\mathbf{r}'). \end{aligned} \tag{3.7}$$

where ϕ is the scalar potential, $\mathbf{A}$ is the vector potential, and the subscript S indicates that the electric field is due to the source only. $\mathbf{J}_S$ and ρ_S are proportional to I_S,

while $\mathbf{J}_D$ is proportional to I_D, so we find that

$$P_{DS} = i\omega_0 M I_S I_D, \tag{3.8}$$

where M, the "effective inductance" is a function of ω_0 and the geometry of the system. We then conclude from standard coupled-mode theory arguments and a comparison with Eq. 2.2 that $\kappa = \omega_0 M/2\sqrt{L_S L_D}$.

3.6 Validity of the quasi-static approximation

So far, we have worked in the quasi-static approximation and treated the interaction between the two coils as instantaneous. The quasi-static approximation is good as long as $\omega_0 D/c \ll 1$, where D is the distance between the source and device, the longest dimension in our system. In the lab, we worked with frequencies of about 10MHz and distances of up to 2.5m, for which $\omega_0 D/c \simeq 0.5$. Thus, we need to justify the quasi-static approximation more carefully.

The most significant corrections to the quasi-static regime would affect κ, since it is the only coupled-mode theory parameter which depends on the distance between the coils. If this quantity is affected considerably, then the coupled-mode analysis would be more complicated because of the non-instantaneous interaction. To quantify the change in κ, we need to replace the instantaneous potentials in the second line of Eq. 3.7 by the retarded potentials

$$\begin{aligned} \phi_S(\mathbf{r},t) &= \frac{1}{4\pi\epsilon_0}\int d\mathbf{r}' \frac{\rho_S(\mathbf{r}',t)e^{i\omega_0|\mathbf{r}'-\mathbf{r}|/c}}{|\mathbf{r}'-\mathbf{r}|}, \\ \mathbf{A}_S(\mathbf{r},t) &= \frac{\mu_0}{4\pi}\int d\mathbf{r}' \frac{\mathbf{J}_S(\mathbf{r}',t)e^{i\omega_0|\mathbf{r}'-\mathbf{r}|/c}}{|\mathbf{r}'-\mathbf{r}|}, \end{aligned} \tag{3.9}$$

where we have used the Lorenz gauge. We have explicitly computed these corrections by numerical integration and found that they are within the error bars due to uncertainties in the measurement of the geometrical dimensions. Therefore the quasi-static approximation is valid for our purposes.

Chapter 4

Finite element analysis of the resonators

4.1 Overview

In an attempt to check and improve upon the analytical model introduced in the previous chapter, we modeled both isolated and coupled self-resonant coils using the RF module of the COMSOL Multiphysics finite element analysis software. The basic idea of finite element analysis is to discretize the system into a mesh of subdivisions (hence finite element) and nodes. The nodes represent the degrees of freedom, and each element is associated with a number of nodes. A physical quantity at an arbitrary point in a given finite element is approximated by interpolation (with a suitable function) from its values at the nodes associated with that element. The physical equations governing the system are then used in conjunction with the interpolating functions to determine a system of equations for an element in term of its nodal degrees of freedom. The equations for different elements are then combined into a set of equations describing the entire system, and these are then solved with the appropriate boundary conditions.

The finite element analysis of the self-resonant coils is complicated by the lack of symmetries of the coils which, if present, could have been used to significantly reduce the number of degrees of freedom that need to be solved. Nevertheless, the current

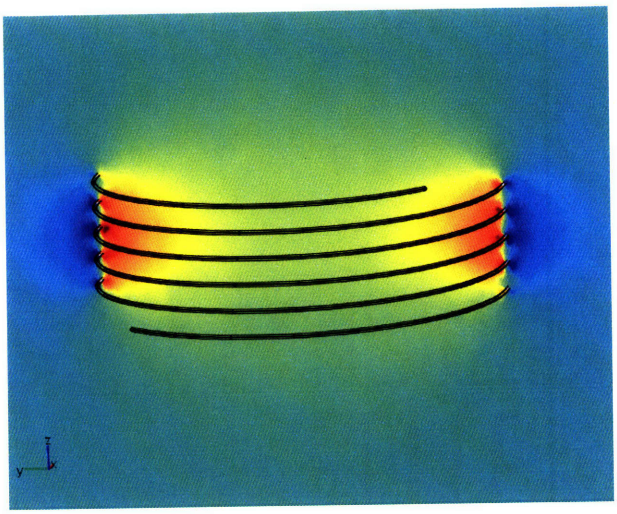

Figure 4-1: Lowest eigenmode of a self-resonant coil, simulated with COMSOL Multiphysics. The colormap represents the z-component of the magnetic field.

results are encouraging and it is probable that given a relatively modest increase in computational power we should be able to extract precise values for all coupled-mode theory parameters from these simulations.

4.2 A single isolated coil

Solving for the eigenvalue of a self-resonant coil allows us to determine both its eigenfrequency f_0 and its loss rate Γ (or, equivalently, Q). We performed this analysis in two steps. First, we solved for the eigenvalue of a coil made of perfect conductor (i.e. we imposed perfect electric conductor boundary conditions at its surface), then we repeated the procedure for a coil made of copper (by switching to impedance boundary conditions). The first step serves two purposes: it yields the radiative quality factor Q_r and it determines the minimum distance necessary between the coil and the outer boundary of the physical space being modeled. We chose this outer boundary to be a sphere, and applied scattering boundary conditions to it, in order to prevent reflections back towards the coil. If the radius of this outer sphere is too small and the boundary is too close to the coil, it will damp the oscillations of the coil and affect its eigenfrequency. Thus, we know we have chosen an appropriate radius for the outer

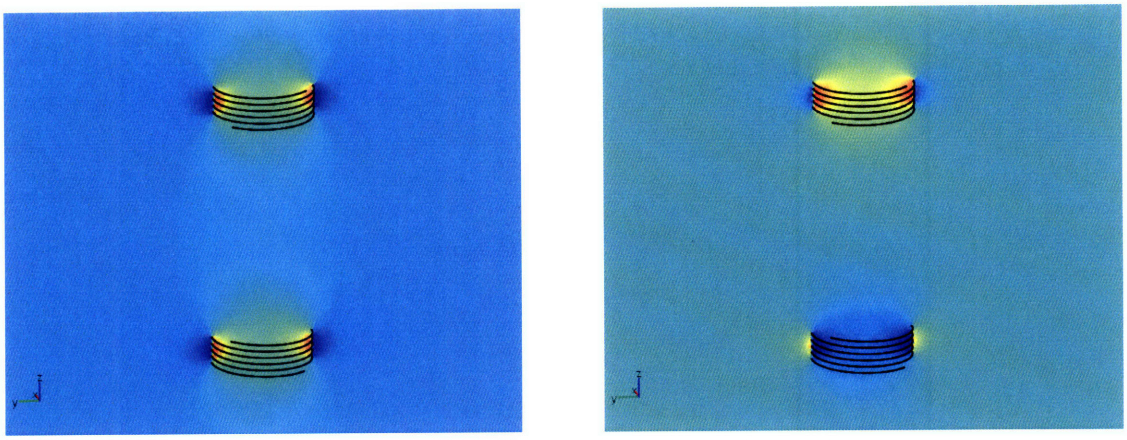

Figure 4-2: Even (left) and odd eigenmodes of two coupled self-resonant coils. The colormap represents the z-component of the magnetic field.

boundary when a further increase in radius does not change the eigenfrequency. The eigenvalue of the coil with impedance boundary conditions determines the total Q, from which we may obtain the ohmic quality factor through $Q_o^{-1} = Q^{-1} - Q_r^{-1}$.

Although we had to limit the simulations (Fig. 4-1) to somewhat coarse discretizations, the values for f_0 and Q that we obtained are probably quite precise: between the finest mesh for which we could solve and the next finest, there was only a 1% discrepancy in f_0, and a 2% discrepancy in Q.

4.3 Two coupled coils

As shown in Eq. 2.8, one can derive the coupling κ from the splitting between the eigenfrequencies of two coupled resonators. Since the two coils are identical, we can exploit this symmetry and reduce the number of nodal degrees of freedom that need to be solved for. By imposing perfect electric conductor and perfect magnetic conductor boundary conditions at the plane of reflection between the two coils, we can respectively solve for the odd and even modes of the coupled system.

Unfortunately, the frequency splitting is much smaller than the eigenfrequencies themselves, and the latter would have to be precise to nearly one part per thousand in order to reliably estimate κ. Even when taking advantage of the reduction in the size of the system afforded by reflection symmetry, we were unable perform the finite

element analysis for a mesh that was sufficiently fine to attain this level of precision. Nonetheless, the modes exhibit the expected qualitative behavior even at coarser discretizations (Fig. 4-2).

Chapter 5

Comparison of theory with experimental parameters

5.1 Frequency and quality factor

The geometrical dimensions for the two identical helical coils built for the experimental validation of the power transfer scheme are $h = 20$cm, $a = 3$mm, $r = 30$ cm, and $n = 5.25$. Both coils are made of copper. For these parameters, our analytical model predicts $f_0 = 10.52$MHz, $Q = 2,500$, $Q_o = 3,100$, and $Q_r = 13,100$, while the finite element modeling yields $f_0 = 9.93$MHz, $Q = 2,020$, $Q_o = 2,350$, and $Q_r = 14,500$. The resonant frequency and quality factor are measured experimentally by driving the self-resonant coil with a coil connected to a function generator and measuring the amplitude of the self-resonant coil's excitation with a pickup coil connected to an oscilloscope (Fig. 5-1). To ensure that the driving and pickup coils do not load the resonator and interfere with the measurement, we placed them at a sufficient distance from it (we found 30cm to be enough). This experimental setup corresponds to the case treated in Sec. 2.2.

We measured $f_0 = 9.90$MHz and $Q = 950 \pm 50$. The frequency obtained from the finite element analysis agrees remarkably well with the experimental result, while the frequency predicted by the analytical model is just over 5% above the experimental. On the other hand, the experimental Q is much below either theoretical prediction.

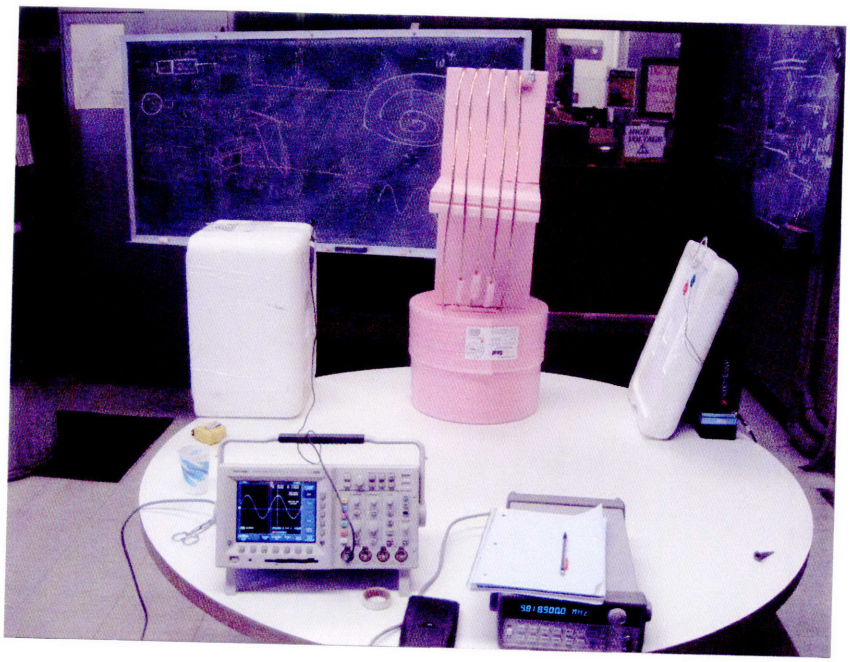

Figure 5-1: Experimental setup for measuring Q. The self-resonant coil is the copper wire wrapped around the piece of pink styrofoam. The excitation coil to its right is connected to a function generator, while the pickup coil on the opposite side is connected to the oscilloscope.

We believe this discrepancy is mostly due to the effect of the layer of poorly conducting copper oxide on the surface of the copper wire, to which the current is confined by the short skin depth ($\sim 20\mu$m) at this frequency. Although the two theoretical Q_r's agree reasonably well, there is a substantial disagreement between the Q_o's. This may be due in large part because we ignored in our analytical model the power dissipated by the eddy currents that a loop of the self-resonant coil induces on its neighbors.

Because of the significant mismatch between the experimental and theoretical Q's, we shall use the experimentally observed Q and $\Gamma_S = \Gamma_D = \Gamma = \omega/2Q$ derived from it in all subsequent computations.

5.2 Coupling coefficient

To measure the coupling κ, we place the two self-resonant coils (fine-tuned, by slightly adjusting h, to the same resonant frequency when isolated) a distance D apart then

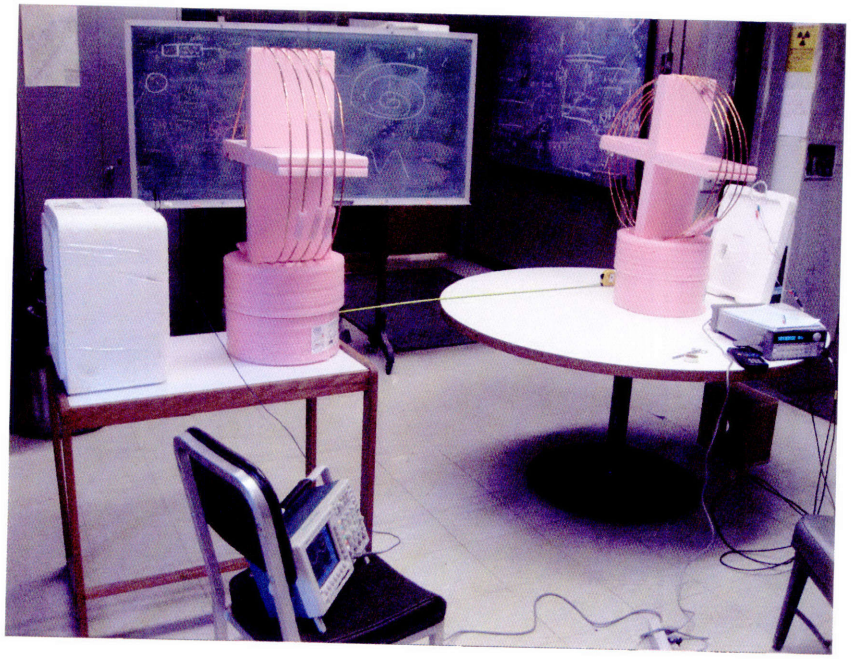

Figure 5-2: Experimental setup for measuring κ. The self-resonant coil on the right-hand side is driven by a coil connected to a function generator. A pickup coil measures the amplitude of the excitation in the second coil.

excite one of them while measuring the amplitude of the excitation in the second coil. This is precisely the setup described by Eq. 2.10, and κ is related to the frequency splitting between the two peaks measured at the second coil by $\Delta\omega = 2\sqrt{\kappa^2 - \Gamma^2}$. Although our focus in these experiments is on the case where the two coils are aligned coaxially (Fig. 5-3), we obtain similar results for κ vs. distance for other orientations (Figs. 5-4 and 5-5).

5.3 Range of the strong coupling regime

As we showed in Ch. 3, κ and Γ are both functions of the frequency: κ is roughly proportional to ω, while Γ is affected by ohmic losses (which scale as $\omega^{1/2}$ because of the skin effect), radiation losses (whose electric and magnetic dipole components scale as ω^2 and ω^4 respectively), and possibly also by eddy current losses (which are proportional to ω^2). Because of these competing physical effects, κ/Γ and the efficiency are maximized for a particular value of f. Our experience with simulations

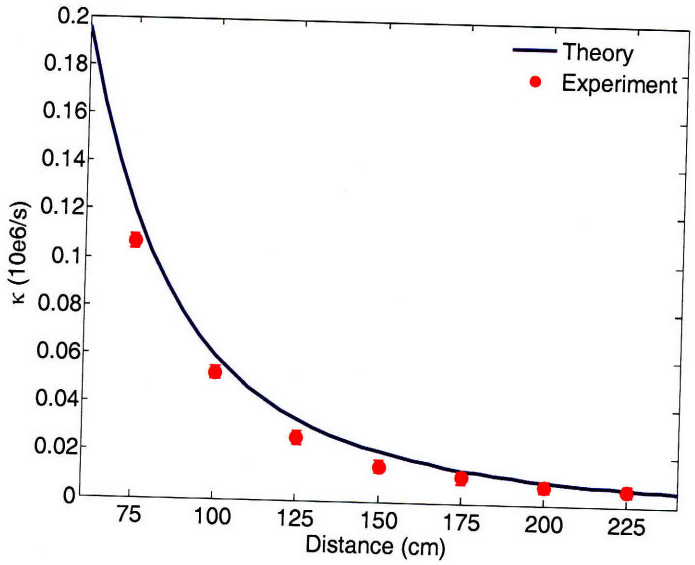

Figure 5-3: Comparison of experimental and theoretical values for κ as a function of the separation between coaxially aligned source and device coils (the wireless power transfer distance). Note that when the distance D between the centers of the coils is much larger than their characteristic size, κ scales with the D^{-3} dependence characteristic of dipole-dipole coupling.

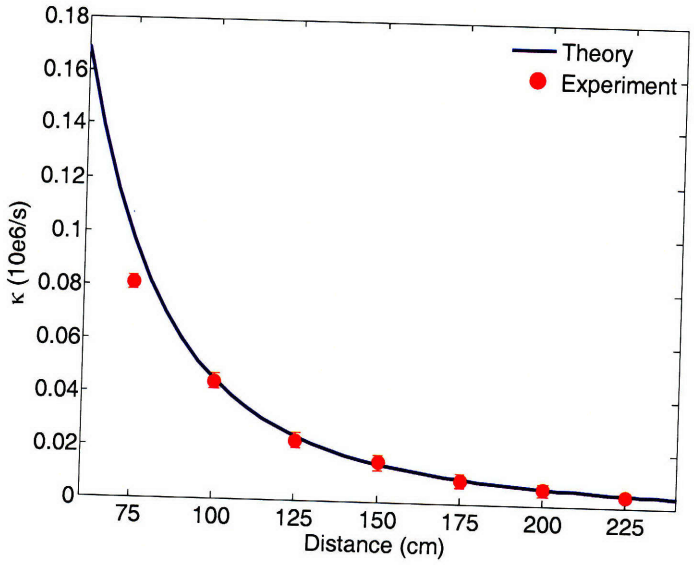

Figure 5-4: Theoretical and experimental κ as a function of distance when one of the coils is rotated by 45% with respect to coaxial alignment.

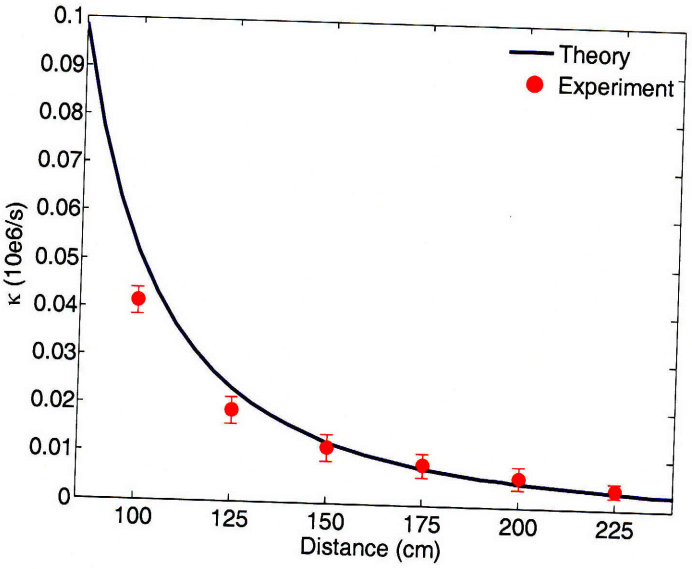

Figure 5-5: Theoretical and experimental κ as a function of distance when the coils are coplanar.

shows that this optimal frequency is in the range $1 - 25$MHz for typical parameters of interest and that picking an appropriate frequency for a given coil geometry plays a major role in maximizing the power transfer. Because of the discrepancy between the predicted and measured Q, however, we were unable to use theory to determine the ideal frequency of operation for our coils. Instead, we relied on educated guesses and some trial and error in the laboratory. Thus, although the coils were in the strong coupling regime throughout the range of distances probed (Fig. 5-6), a better understanding of the loss mechanisms would enable us to better fine-tune the system and improve performance.

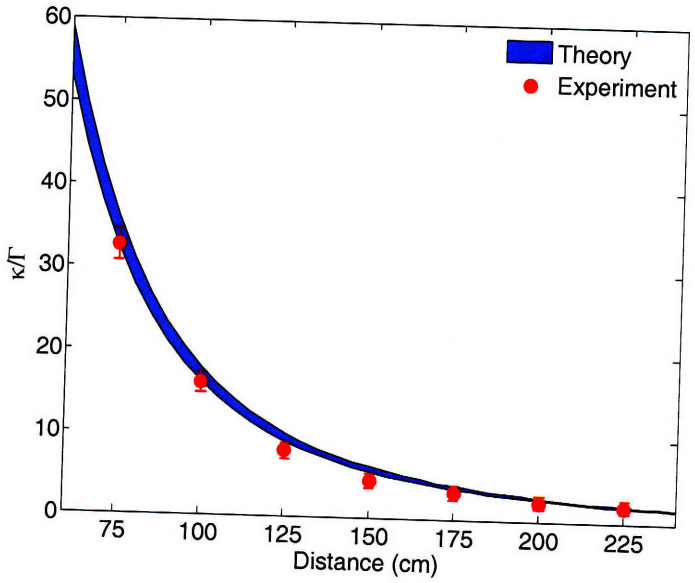

Figure 5-6: Comparison of experimental and theoretical values for the parameter κ/Γ as a function of the wireless power transfer distance. The theory values are obtained by using the theoretical κ and the experimentally measured Γ. The shaded area represents the spread in the theoretical κ/Γ due to the $\pm 5\%$ uncertainty in Q.

Chapter 6

Measurement of the efficiency

6.1 Description of the setup

As the circuit driving the entire apparatus, we use a standard Colpitts oscillator whose inductive element consists of a single loop of copper wire 25cm in radius(Fig. 6-1); this loop of wire couples inductively to the source coil and drives the entire wireless power transfer apparatus. The load consists of a calibrated light-bulb, and is attached to its own loop of insulated wire, which is placed in proximity of the device coil and inductively coupled to it. [1] By varying the distance between the light-bulb and the device coil, we are able to adjust the parameter Γ_W/Γ so that it matches its optimal value, given theoretically by $\sqrt{1+\kappa^2/\Gamma^2}$. (The loop connected to the light-bulb adds a small reactive component to Γ_W which is compensated for by slightly retuning the coil.) We measure the work extracted by adjusting the power going into the Colpitts oscillator until the light-bulb at the load glows at its full nominal brightness.

6.2 Results

We determine the efficiency of the transfer taking place between the source coil and the load by measuring the current at the mid-point of each of the self-resonant coils

[1] The couplings to the driving circuit and the load do not have to be inductive. They may also be connected by a wire, for example. We have chosen inductive coupling in the present work because of its easier implementation.

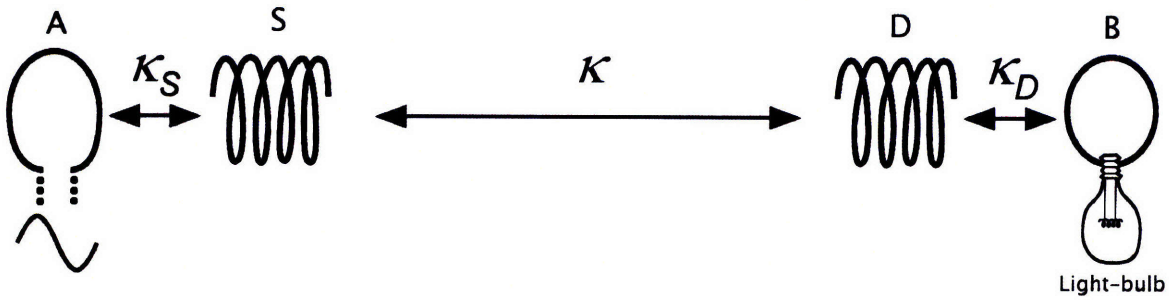

Figure 6-1: Schematic of the experimental setup. A is a single copper loop of radius 25cm that is part of the driving circuit, which outputs a sine wave with frequency 9.9MHz. S and D are respectively the source and device coils referred to in the text. B is a loop of wire attached to the load ("light-bulb"). The various κ's represent direct couplings between the objects indicated by the arrows. The angle between coil D and the loop A is adjusted to ensure that their direct coupling is zero, while coils S and D are aligned coaxially. The direct couplings between B and A and between B and S are negligible.

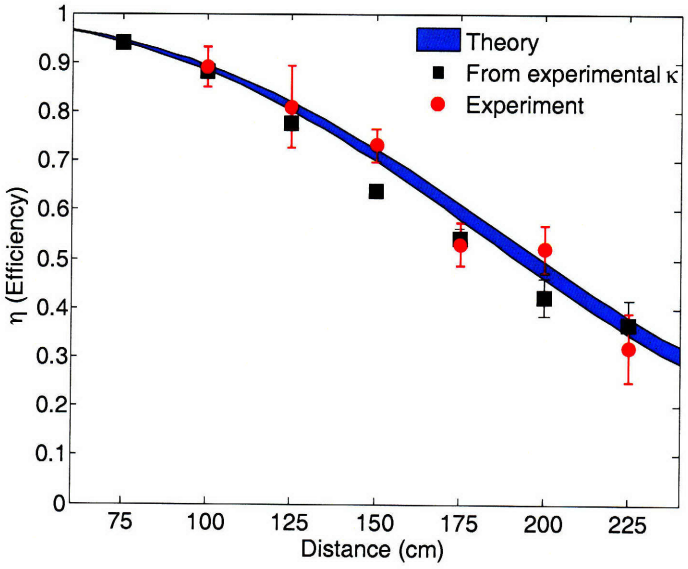

Figure 6-2: Comparison of experimental and theoretical efficiencies as functions of the wireless power transfer distance. The shaded area represents the theoretical prediction for maximum efficiency, and is obtained by inserting the theoretical values from Fig. 5-6 into Eq. 2.12 (with $\Gamma_W/\Gamma_D = \sqrt{1+\kappa^2/\Gamma^2}$.) The black dots are the maximum efficiency obtained from Eq. 2.12 and the experimental values of κ/Γ from Fig. 5-6. The red dots present the directly measured efficiency, as described in the text.

with a current-probe (which does not lower the Q of the coils noticeably). This gives a measurement of the current parameters I_S and I_D used in our theoretical model. We then compute the power dissipated in each coil from $P_{S,D} = \Gamma L |I_{S,D}|^2$, and obtain the efficiency from $\eta = P_W/(P_S+P_D+P_W)$. To ensure that the experimental setup is well described by a two-object coupled-mode theory model, we position the device coil such that its direct coupling to the copper loop attached to the Colpitts oscillator is zero. The experimental results are shown in Fig. 6-2, along with the theoretical prediction for maximum efficiency, given by Eq. 2.12. We are able to transfer significant amounts of power using this setup, fully lighting up a 60W light-bulb from distances more than 2m away.

As a cross-check, we also measure the total power going from the wall power outlet into the driving circuit. The efficiency of the wireless transfer itself is hard to estimate in this way, however, as the efficiency of the Colpitts oscillator itself is not precisely known, although it is expected to be far from 100% [18]. Still, the ratio of power extracted to power entering the driving circuit gives a lower bound on the efficiency. When transferring 60W to the load over a distance of 2m, for example, the power flowing into the driving circuit is 400W. This yields an overall wall-to-load efficiency of 15%, which is reasonable given the expected efficiency of roughly 45% for the wireless power transfer at that distance and the low efficiency of the Colpitts oscillator.

Chapter 7

Practical issues

7.1 Robustness of the strong coupling regime

It is essential that the coils be on resonance for the power transfer to be practical [8]: we estimate that given the parameters of our system, the efficiency of an off-resonant system would be suppressed by a factor of approximately $1/Q^2 \sim 10^6$. Experimentally, we find that the power transmitted to the load drops sharply as either one of the coils is detuned from resonance. For a fractional detuning $\Delta f/f_0$ of a few times Q^{-1}, the induced current in the device coil is indistinguishable from noise. Although we were able to tune the coils manually with only a moderate amount of effort, a practical system would need a feedback mechanism that would tune it automatically.

A detailed and quantitative analysis of the effect of external objects on our scheme is beyond the scope of the current work, but we would like to note here that, confirming our intuition that off-resonant objects couple relatively weakly, the power transfer is not visibly affected as humans and various everyday objects, such as metals, wood, and electronic devices large and small, are placed between the two coils, even in cases where they completely obstruct the line of sight between source and device (Fig. 7-1). External objects have a noticeable effect only when they are within a few centimeters from either one of the coils. While some materials (such as aluminum foil, styrofoam and humans) mostly just shift the resonant frequency, which can in principle be easily

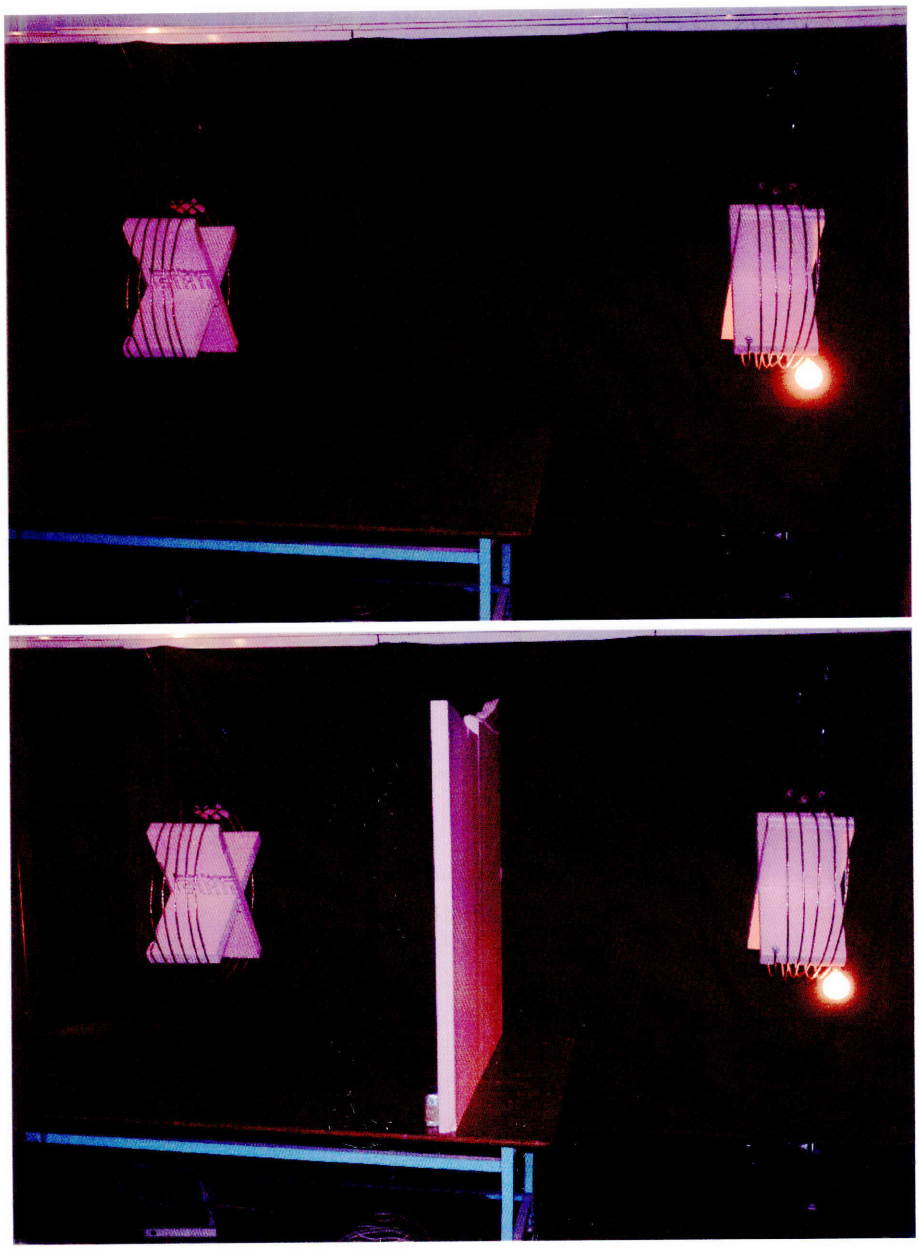

Figure 7-1: 60W light-bulb being lit from 2m away. Note the obstruction in the lower image.

corrected with a feedback circuit, others (cardboard, wood, and PVC) lower Q when placed closer than a few centimeters from the coil, thereby lowering the efficiency of the transfer.

7.2 Safety and interference concerns

When transferring 60W across 2m, we calculate that at the point halfway between the coils the RMS magnitude of the electric field is $E_{rms} = 210\text{V/m}$, that of the magnetic field is $H_{rms} = 1\text{A/m}$, and that of the Poynting vector is $S_{rms} = 3.2\text{mW/cm}^2$.[1] These values increase closer to the coils, where the fields at source and device are comparable. For example, at distances 20cm away from the surface of the device coil, we calculate the maximum values for the fields to be $E_{rms} = 1.4\text{kV/m}$, $H_{rms} = 8\text{A/m}$, and $S_{rms} = 0.2\text{W/cm}^2$. The power radiated for these parameters is approximately 5W, which is roughly an order of magnitude higher than cell phones. In the particular geometry studied in this article, the overwhelming contribution (by one to two orders of magnitude) to the electric near-field, and hence to the near-field Poynting vector, comes from the electric dipole moment of the coils. If instead one uses a capacitively-loaded single-turn loop design [8] - which has the advantage of confining nearly all of the electric field inside the capacitor - and tailors the system to operate at lower frequencies, it should be possible to reduce the values cited above for the electric field, the Poynting vector, and the power radiated to below general safety regulations [19].

f_0(MHz)	η	E_{rms} (V/m)	H_{rms} (A/m)	S_{rms}(W/cm^2)	Power radiated (W)
10	83%	185	21	0.08	3.3
1	60%	40	14	0.04	0.005

Table 7.1: Effect of replacing self-resonant coils with capacitively-loaded loops and of lowering the resonant frequency on electromagnetic fields 20cm away from the surface of the device loop. The power radiated by the system is also shown. The total power transferred is 60W.

We have performed calculations to simulate a transfer of 60W across two identical capacitively-loaded loops similar in dimension to our self-resonant coils (radius of loop 30cm, cross sectional radius of the conductor 3cm, and distance between the loops of 2m), and calculated the maximum values of the fields and Poynting vector 20cm away from the device loop (Table 7.1). At 1MHz, all our fields are below the IEEE safety guidelines ($E_{rms} = 614\text{V/m}$, $H_{rms} = 16.3\text{A/m}$, and $S_{rms} = 0.1\text{W/cm}^2$) for that

[1]Note that $E \neq c\mu_0 H$, and that the fields are out of phase and not necessarily perpendicular to each other because we are not in a radiative regime.

frequency, and the power radiated is well below the limits for Bluetooth (100mW) and WiFi (100mW or higher, depending on country).

7.3 Directions for future research

Although the two coils are currently of identical dimensions, it is possible to make the device coil small enough to fit into portable devices without decreasing the efficiency. One could, for instance, maintain the product of the characteristic sizes of the source and device coils constant, as argued in [8].

We believe that the efficiency of the scheme and the power transfer distances could be appreciably improved by silver-plating the coils, which should increase their Q, or by working with more elaborate geometries for the resonant objects [20]. Nevertheless, the performance characteristics of the system presented here are already at levels where they could be useful in practical applications.

Bibliography

[1] Nikola Tesla, U.S. patent 1,119,732 (1914).

[2] N. Tesla, *Nikola Tesla: Lectures, Patents, Articles* (Nikola Tesla Museum, Belgrade, 1956), p. A109.

[3] N. Tesla, *Colorado Springs Notes 1899-1900* (Nikola Tesla Museum, Belgrade, 1978).

[4] J. M. Fernandez and J. A. Borras. U.S. patent 6,184,651.

[5] A. Esser and H.-C. Skudelny, IEEE Trans. on industry applications **27**, 872 (1991).

[6] J. Hirai, T.-W. Kim, and A. Kawamura, IEEE Trans. on power electronics **15**, 21 (2000).

[7] T. A. Vanderelli and J. G. Shearer and J. R. Shearer, U.S. patent 7,027,311 (2006).

[8] A. Karalis, J. D. Joannopoulos, and M. Soljačić, Ann. Phys. (2007), 10.1016/j.aop.2007.04.017.

[9] T. Aoki, B. Dayan, E. Wilcut, W. P. Bowen, A. S. Parkins, T. J. Kippenberg, K. J. Vahala, and H. J. Kimble, Nature **443**, 671 (2006).

[10] K. O'Brien, G. Scheible and H. Gueldner, *The 29th Annual Conference of the IEEE* **1**, 367 (2003).

[11] L. Ka-Lai and J. W. Hay and P. G. W. Beart, U.S. patent 7,042,196 (2006).

[12] C. M. Zierhofer and E. S. Hochmair, IEEE Transactions on Biomedical Engineering **37**, 716 (1990).

[13] A. Kurs, A. Karalis, R. Moffatt, J. D. Joannopoulos, P. Fisher, and M. Soljačić, Science **317**, 83 (2007).

[14] H. Haus, *Waves and Fields in Optoelectronics* (Prentice-Hall, New Jersey, USA, 1984).

[15] S. Sensiper, *Electromagnetic Wave Propagation on Helical Conductors*, PhD thesis, Massachusetts Institute of Technology, 1951.

[16] COMSOL Multiphysics RF Module.

[17] J. D. Jackson, *Classical Electrodynamics*, 3rd ed. (Wiley, New York, 1999).

[18] W. A. Edson, *Vacuum-tube oscillators* (Wiley, New York, USA, 1953).

[19] *IEEE Std C95.1 - 2005 IEEE Standard for Safety Levels with Respect to Human Exposure to Radio Frequency Electromagnetic Fields, 3 kHz to 300 GHz*, IEEE, Piscataway, NJ (2006).

[20] J. B. Pendry, Science **306**, 1353 (2004).